

Anisotropic Saturable and Excited-State Absorption in Bulk ReS₂

Xianghai Meng, Yongjian Zhou, Ke Chen, Richard H. Roberts, Wenzhi Wu, Jung-Fu Lin, Ray T. Chen, Xiaochuan Xu, and Yaguo Wang*

The intensity-scan (I-scan) technique to study the polarization-dependent, nonlinear processes in exfoliated bulk ReS₂ is utilized. The polarization-dependent reflection and transmission of ReS₂, from which the absorption coefficients are extracted using the transfer matrix method, are measured. Absorption coefficients under high laser peak power show a transition from saturable absorption (SA) to reverse saturable absorption when rotating the laser polarization with respect to the *b*-axis. It is found that SA and excited-state absorption (ESA) contribute to the nonlinear optical processes. Both the SA and ESA show strong dependence on the polarization angle, which is attributed to the anisotropic optical transition probability and electronic band structure in ReS₂. The anisotropic nonlinear optical properties of ReS₂ may find applications as saturable absorbers in lasers and optical modulators.

1. Introduction

Transition metal dichalcogenides (TMDs), a family of 2D materials, have promising applications in nanoelectronics and optoelectronics due to their extraordinary properties, such as

X. Meng, Y. Zhou, Dr. K. Chen, Prof. Y. Wang
Department of Mechanical Engineering
The University of Texas at Austin
Austin, TX 78712, USA
E-mail: yaguo.wang@austin.utexas.edu


R. H. Roberts, Prof. J.-F. Lin, Prof. Y. Wang
Texas Materials Institute
The University of Texas at Austin
Austin, TX 78712, USA

Prof. W. Wu
School of Electronic Engineering
Heilongjiang University
Harbin 150080, China

Prof. J.-F. Lin
Jackson School of Geosciences
The University of Texas at Austin
Austin, TX 78712, USA

Prof. R. T. Chen
Microelectronics Research Center
Department of Electrical and Computer Engineering
The University of Texas at Austin
Austin, TX 78758, USA

Prof. R. T. Chen, Dr. X. Xu
Omega Optics, Inc.
Austin, TX 78757, USA

 The ORCID identification number(s) for the author(s) of this article can be found under <https://doi.org/10.1002/adom.201800137>.

DOI: 10.1002/adom.201800137

thickness-dependent bandgap,^[1–3] intra- and interlayer excitons,^[4–7] and valley polarization.^[6,8–10] TMDs (chemical formula MX₂) share similar lattice structures, in which one layer of M atoms (transition metal atom, Mo, W, etc.) is sandwiched between two layers of X atoms (chalcogen atom, S, Se, or Te). Individual layers are bonded by weak van der Waals (vdW) forces. In most 2H TMDs, such as MoS₂, WS₂, and MoSe₂, a direct bandgap is only observed at single layer form; when the number of stacked layers increases, they transition into an indirect gap semiconductor and the bandgap drops sharply.^[11,12]

Recently, another member of the TMD family, rhenium disulfide (ReS₂), has begun to attract much attention. Different from the 2H structure of classical TMDs, ReS₂ possesses a distorted 1T triclinic crystal structure, as shown in **Figure 1a**.^[13] The bandgap evolution of ReS₂ is peculiar compared to other 2H TMDs. Dileep et al. and Tongay et al. suggested that bulk and multilayer ReS₂ have direct bandgap^[14,15] and Tongay et al. also observed monolayer behavior in bulk ReS₂ due to the electronic and vibrational decoupling.^[15] However, other studies reported that bulk and multilayer ReS₂ are actually indirect bandgap semiconductors, with band edge around 1.35–1.5 eV.^[16–20] A very recent study by Gehlmann et al., which studied ReS₂ via k-space photoemission microscopy, suggested that only bi-layer ReS₂ is a direct bandgap semiconductor.^[21] Despite these discrepancies, the reported bandgap energy dependence on layer thickness in ReS₂ is much weaker compared with classical TMDs. For multilayer and monolayer ReS₂, though indirect bandgap in nature, the difference of conduction band minimum (CBM) and valence band maximum (VBM) in momentum space is very small compared with other TMDs, which explains why there is no drastic change of photoluminescence (PL) efficiency with reducing layer thickness.

Aside from its unique bandgap behavior, ReS₂ also possesses another prominent feature that distinguishes it from 2H TMDs: in-plane anisotropy. The additional *d* valence electron from Re atoms contributes to the formation of zig-zag Re chains parallel to the *b*-axis of the crystal, which drastically reduces its symmetry and affects its physical properties. The highly anisotropic optical,^[16] vibrational,^[22–25] thermal,^[26] and electronic transport properties^[27] demonstrated in ReS₂ make it promising for applications in sensors and electronic devices,^[17,28] such as polarization-sensitive detectors based on

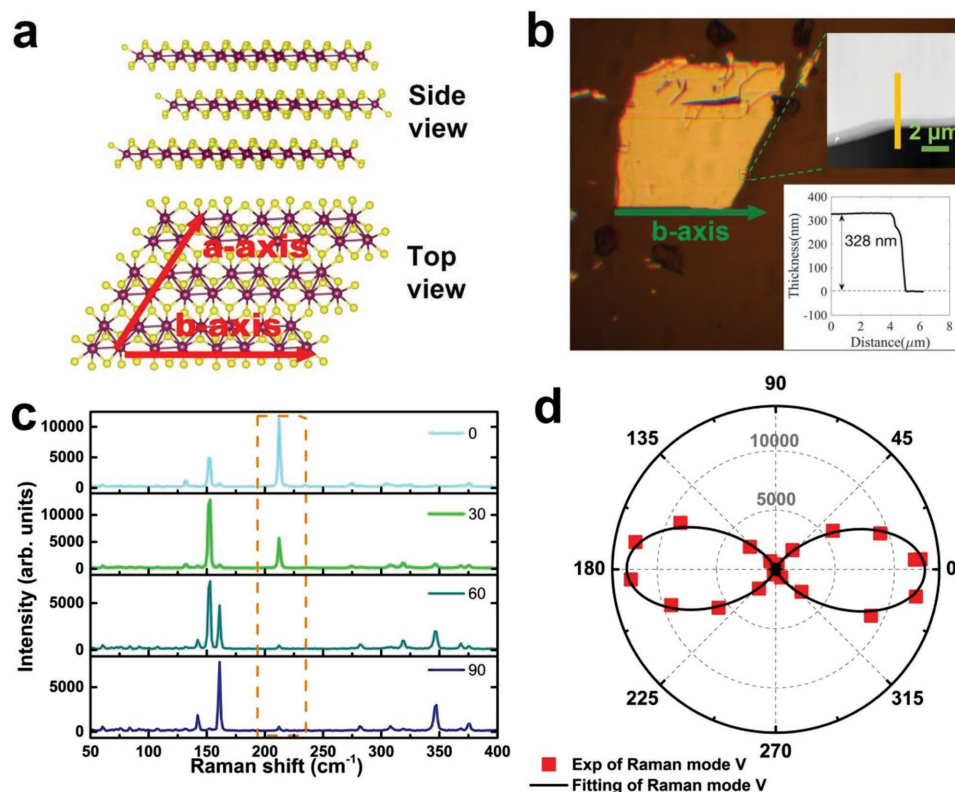


Figure 1. a) Illustration of ReS₂ crystal structure: side view (upper) and top view (bottom), with *a*-axis and *b*-axis marked with red arrows. b) Optical image of bulk ReS₂ sample exfoliated onto thin glass substrate; inset is the thickness measurement by AFM. Green arrow marks the *b*-axis determined by Raman spectroscopy. c) Polarized Raman spectroscopy of ReS₂ sample with parallel polarization for excitation (532 nm) and collection beams at selected polarizations. Mode V, which is used to identify the *b*-axis, is outlined in orange. d) Experimental and fitted result of the intensity of Raman Mode V shown in polar coordinates.

the anisotropic in-plane optical absorption.^[29] Comparing with black phosphorous, whose in-plane anisotropic properties have also been studied,^[30–32] the excitonic and band-edge transitions of ReS₂ have decoupled polarization dependence between the regularly observed Exciton I (1.51 eV) and Exciton II (1.57 eV), allowing for tuning of individual transitions.^[16,33] Furthermore, optical transitions in the near-infrared to visible wavelength region and the environmental stability make ReS₂ more attractive for optoelectronic devices.

In order to implement ReS₂ into optoelectronic applications, a thorough examination of its optical response is essential. Nonlinear optical effects have been reported extensively in classical TMDs,^[34–36] however, very few studies of ReS₂'s nonlinear optical properties have been conducted to date.^[37,38] Cui et al. have measured the different saturation fluence for saturable absorption (SA) in CVD grown multilayer ReS₂ at 1550 nm wavelength,^[37] but only with light polarization parallel and perpendicular to the ReS₂ basal plane, so the in-plane anisotropy is not considered. Cui et al. (a different group) have derived the third-order nonlinear optical susceptibility $|\chi^3|$ of monolayer and multilayer ReS₂ ($\approx 10^{-18}$ m² V⁻²) based on the third harmonic oscillation (THG) and found that the intensity of THG depends on the incident light polarization.^[38]

The Z-scan technique is used as a standard method to study the nonlinear optical response,^[39] where the incident laser power is fixed and the irradiance on the sample is changed by

scanning the sample position around the laser focal point. In the standard Z-scan technique, a large sample size and good sample homogeneity are required. As a result, most Z-scan experiments in TMDs are conducted in solutions with suspended TMD nanoflakes,^[40–42] from which it is difficult to resolve the polarization-dependent response. With the intensity-scan (I-scan) technique, where the laser irradiance is controlled by neutral density filters instead of moving the sample position, one can determine the nonlinear optical properties in inhomogeneous samples with low damage threshold.^[43–45] Thus, the I-scan technique is much better suited to study exfoliated or CVD-grown, single-domain 2D flakes, which usually have a very limited radiation area.^[46]

In this paper, we have studied the anisotropic nonlinear optical properties in exfoliated bulk ReS₂ with the I-scan technique (please see the Supporting Information for the I-scan experimental setup). Our photon energy (1.57 eV) is set to resonate with Exciton II to reveal its anisotropic nonlinear properties. By simultaneously measuring the polarization-dependent transmission and reflection, the real and imaginary parts of complex refractive index have been extracted using the transfer matrix method, from which we obtain the absorption coefficients. The coefficient of both the linear and nonlinear absorption shows clear anisotropic behavior. More interestingly, we observe a transition from SA to reverse saturable absorption (RSA) with polarization angle, which can be attributed to the

anisotropic saturable absorption and excited-state absorption (ESA) in bulk ReS₂.

2. Results and Discussion

The ReS₂ sample was prepared via mechanical exfoliation with scotch tape from bulk crystal (purchased from 2D Semiconductors), and then transferred onto a thin glass substrate (180 μm). The sample thickness was about 328 nm, which was measured with atomic force microscopy (AFM) as shown in the inset of Figure 1b. Due to the stronger bonding between Re–Re atoms along *b*-axis, the crystal preferentially breaks along this direction and the crystal orientation of ReS₂ can be easily determined by the long cleaved edge. However, this method alone cannot be applied to determine the orientation of our sample with irregular edges. Therefore, we employ polarized Raman spectroscopy to resolve the crystal orientation by fitting the angle-dependent intensity of Mode V with the equation: $I = a + b\cos^2(\theta - \theta_{\max})$, where *a* and *b* are constants, *I* is the Raman intensity under parallel excitation and collection configuration, and θ is the angle between laser polarization and *b*-axis.^[47] Figure 1c shows the polarized Raman spectrum for parallel excitation and collection beams at selected polarization

angles. The intensity variation of Mode V at $\approx 212\text{ cm}^{-1}$ is fitted with the above equation, as shown in polar coordinates in Figure 1d. The *b*-axis aligns with the direction where the intensity of Mode V is maximized,^[47] which is marked by the green arrow in Figure 1b. Our PL measurements (see Figures S2 and S3, Supporting Information) reveal the indirect bandgap around 1.4 eV,^[16] Exciton I around 1.47 eV, and Exciton II around 1.57 eV. The photon energy is centered at 1.57 eV (790 nm) to resonate with Exciton II.

Before studying the nonlinear optical absorption, the anisotropic linear absorption of ReS₂ is worth studying. We perform simultaneous measurements of reflection and transmission at constant incident energy at 30 μW (peak power 1.55 GW cm⁻² with 1/e² beam radius of 19 μm). The peak power is low enough to make sure nonlinear optical effect does not occur. Figure 2a–c shows the reflectance (*R*), transmittance (*T*), and absorbance (1–*R*–*T*) at different polarization angles with 15° increment. The polarization angle is defined to be the angle between laser polarization and the *b*-axis. All the three quantities show obvious angle-dependent behavior and can be fitted with the same equation as in the Raman intensity of Mode V.^[16] In Figure 2a, the reflectance is maximized at 0° and minimized at 90°. This phenomenon suggests that the effect of the anisotropic linear reflection should be considered in studying the

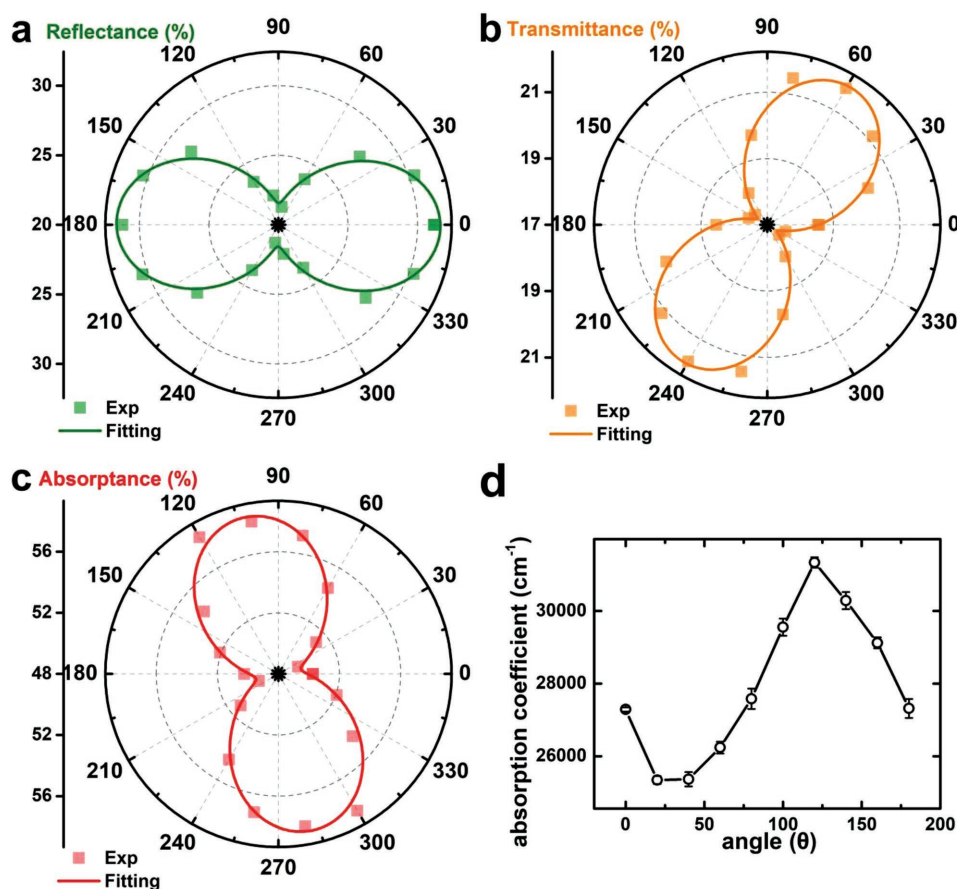


Figure 2. Linear a) reflectance, b) transmittance, and c) absorbance versus polarization angle with respect to the *b*-axis in polar coordinates (squares are experimental data and lines are fitted result). d) Linear absorption coefficient versus polarization angle with respect to the *b*-axis (error bars are standard deviation measured at three spots on the same sample).

nonlinear effect. As shown in Figure 2b, the transmittance shows a minimum around 147° and a maximum around 57° . With both reflectance and transmittance, we derived the linear absorptance simply with $(1-R-T)$, as shown in Figure 2c, where the minimum and maximum absorptance appear at 13° and 102° , respectively. Even though the anisotropic linear absorption in ReS_2 has been reported in previous studies, the observed dependence on polarization angle is inconsistent. For example, Ho et al. observed a maxima of linear absorption at the indirect band edge when the light polarization aligns parallel to the b -axis.^[48,49] Liu et al. reported that the maximum absorption occurs with light polarization perpendicular to b -axis over a broad spectrum (1.55–2.76 eV).^[29] Also, Sim et al. found that the absorption extrema at two exciton energies (1.53 and 1.59 eV) are not aligned with either of the orthogonal directions of b -axis, but at 19° and 87° , respectively.^[33] The possible reason of the discrepancy observed in the anisotropic linear absorption could be the difference in the stacking order of ReS_2 layers. Raman measurements show that the stacking of ReS_2 could be either anisotropic (AA stacking, which results in two interlayer shear Raman modes) or isotropic (AB stacking, which results in two interlayer shear Raman modes).^[50] In multilayer ReS_2 , the stacking could be a combination of AA and AB stacking orders.

With known sample thickness and absorptance, the anisotropic absorption coefficient for our laser wavelength (790 nm) can be deduced with the transfer matrix method. This method is employed here due to the fact that our sample thickness is on the same order of the laser wavelength. In the thin multilayer sample, the Fresnel equations are no longer accurate in deriving the complex refractive index, because the reflection/transmission at multilayer interface will interfere with each other. This interference causes oscillations in the reflection/transmission with respect to laser wavelength or sample

thickness. The transfer matrix method considers the reflection and transmission at each interface and the light propagation in individual layers, thus the complex refractive index can be deduced accurately with the consideration of wavelength and sample geometry (details about derivation of transfer matrix method can be found in the Supporting Information).^[51] The imaginary part of the complex refractive index, k , can be directly linked to the absorption coefficient α ($\alpha = 4\pi k/\lambda$, where λ is the laser wavelength), which we found to vary between 25 000 and 31 000 cm^{-1} , values smaller than but on the same order of magnitude as those reported in literature.^[52,53]

In order to investigate the nonlinear absorption, the incident laser peak power is increased to 72.8 GW cm^{-2} (laser power = $1446 \mu\text{W}$), and the absorptance in linear regime and nonlinear regime are compared, as shown in Figure 3a. The absorptance at high peak power regime also depends on light polarization, and its absolute value (orange curve) follows a similar trend to that at low peak power (blue curve). However, there are two crossing points between these two curves indicating the deviation from linear absorption at high peak power, which is more obvious by plotting the ratio between them (normalized absorptance), as shown in Figure 4b. A ratio less than 1 indicates SA and a ratio greater than 1 indicates RSA. The nonlinear absorption at high peak power shows RSA at 0° (along b -axis), then gradually transits to SA, reaching its peak around 100° before eventually returning to RSA. To further investigate this peculiar transition of nonlinear absorption with polarization angle, we performed I-scan measurements at different polarization angles ranging from 100° to 180° , as shown in Figure 4a. To obtain accurate results of nonlinear absorption, we dropped the assumption that reflection does not change significantly with laser intensity, which has been routinely used in Z-scan and I-scan measurements. Instead, both the

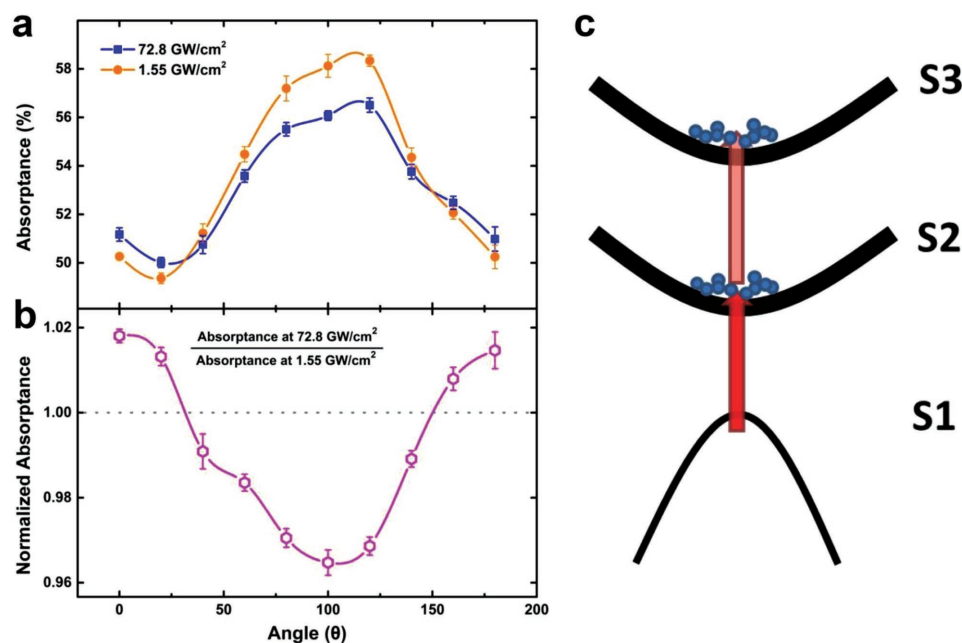


Figure 3. a) Polarization-dependent linear and nonlinear absorption at 1.55 and 72.8 GW cm^{-2} , respectively. b) Polarization-dependent normalized absorption (error bars are standard deviation measured at three spots on the same sample). c) Schematic of excited-state absorption in ReS_2 .

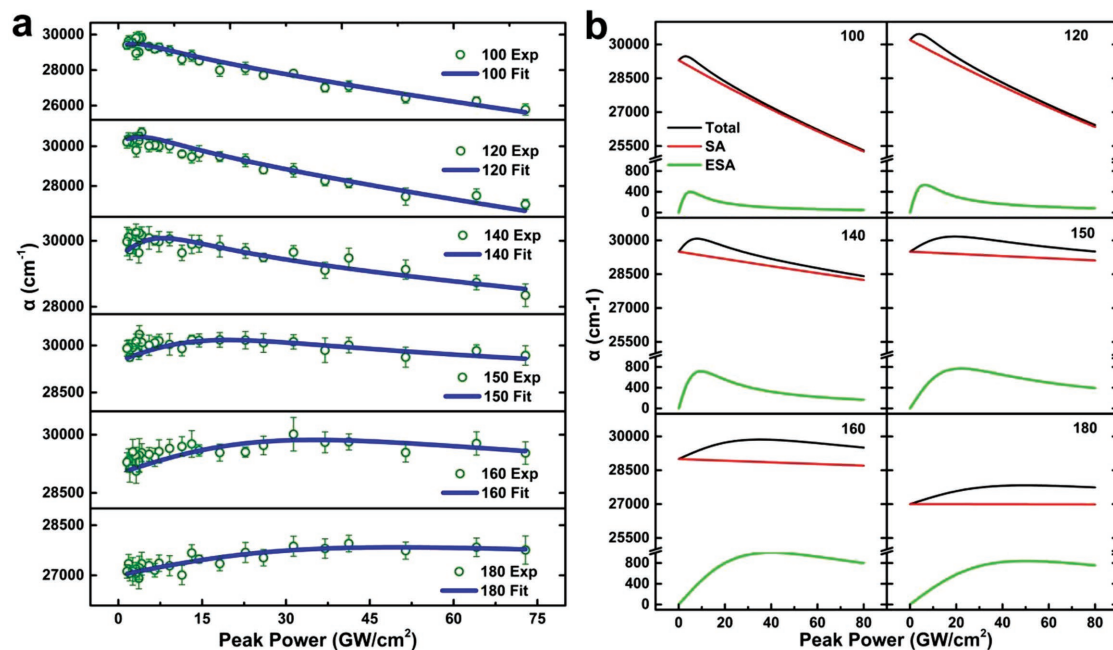


Figure 4. a) Experimental and fitted results of I-scan measurement at different polarization angles (error bars are standard deviation measured at three spots on the same sample). b) Contributions of saturable and excited-state absorption to the total absorption.

reflection and transmission are recorded simultaneously to extract absorption, and then transfer matrix method is applied to obtain the absorption coefficient as in linear absorption case. In Figure 4a, the extracted absorption coefficients (green circles) are plotted as a function of laser peak power at different polarization angles. At 100°, the absorption decreases monotonically with laser peak power, suggesting strong SA. As the polarization angle increases, especially when larger than 140°, a protrusion starts to rise at low peak power regime—which is a sign of RSA—and gradually moves to the high peak power regime with broader power range. Eventually, RSA dominates over SA at 180°.

The mechanism of SA is universal: at high incident power, due to the state filling effect at CBM or the depletion of electrons at VBM, extra photons could not induce additional carrier excitation from conduction band to valence band, resulting in a decrease in absorption.^[54] The physics of RSA is much more complicated and may originate from different mechanisms, such as free carrier absorption (FCA), two-photon absorption (TPA), or ESA.^[54,55] FCA requires preexisting electrons at the CBM (or holes at the VBM). Our ReS₂ sample is undoped with negligible amount of impurities, so the background carrier density is extremely small. Moreover, FCA is an intraband absorption process and involves momentum change of excited carriers. Considering the small momentum that photons can carry, FCA needs the assistance of phonons or impurities to conserve the momentum.^[55] The efficiency of transitions involving multiple particles processes is inherently low. All these factors suggest that FCA can be safely neglected. TPA is responsible for the nonlinear optical phenomena observed in many 2D materials.^[56–58] In black phosphorous, a similar SA to RSA transition with polarization angle is observed.^[59] At certain polarization, the absorption of black phosphorous first decreases with

power because of SA, then increases at high peak power—a feature of TPA. TPA is related to the third-order nonlinear susceptibility term. For most materials, the TPA absorption cross section is small and high laser intensity is required. As a result, TPA is usually observed at high peak power. However, the RSA behavior observed in our experiments appears at low peak power, which is unlikely to be a result of TPA. Therefore, we propose ESA to be a possible mechanism. ESA has been studied vigorously in laser gain media.^[60–63] ESA requires existence of higher-energy excited states that can induce transition between low-lying and high-lying excited states without momentum change.^[64,65] As shown in Figure 3c, the simplest case of ESA involves a three-energy-level system, S1 (ground state), S2 (first excited state), S3 (second excited state). In previous studies, excited (Rydberg) excitonic states of ReS₂ have been observed in the absorption and photoconductivity spectra,^[16,17] which strongly suggests the likelihood of ESA to occur. To observe ESA experimentally, two conditions must be satisfied: the first requirement is that the photon energy has to be resonant with a specific direct transition so that substantial amount of carriers can be excited to state S2, which serves as the “ground state” for transition from S2 to S3.^[54] Our PL measurement (Figure S1, Supporting Information) shows that our laser photon energy (1.51–1.59 eV, centered at 1.57 eV) is resonant with one of the exciton transitions at 1.57 eV from the ground state to S2. Hence, the first requirement is satisfied. The second requirement is that the laser pulse width should be shorter than the relaxation time of excited carrier on state S2, which ensures there is sufficient time to excite carriers from S2 to S3. The pulse width of our femtosecond laser is about 350 fs (FWHM) at the sample position. The exciton recombination time of ReS₂ is reported to be more than 10 ps,^[53] much longer than our laser pulse width. Therefore, the second requirement

is also satisfied. To some extent, ESA is similar to TPA. The major difference between ESA and TPA is that no eigenstate exists at S2 for TPA; instead, S2 of TPA is a virtual state at which the carrier lifetime is extremely short (about fractions of 10^{-15} s).^[54]

Since an optical transition is possible for both $S1 \rightarrow S2$ and $S2 \rightarrow S3$, both the absorption and saturation of S2 and S3 states needs to be considered. Taking into account the effects from both SA and ESA,^[54,55,66] we construct an analytical model to fit the peak power-dependent absorption coefficient at various polarization angles

$$\alpha = \frac{\alpha_0}{1 + \frac{I}{I_{\alpha, \text{sat}}}} + \frac{\beta_0 I}{1 + \left(\frac{I}{I_{\beta, \text{sat}}}\right)^2} \quad (1)$$

where α is absorption coefficient, α_0 is linear absorption coefficient at low peak power, β is ESA absorption coefficient, $I_{\alpha, \text{sat}}$ and $I_{\beta, \text{sat}}$ are saturation terms, and I is the peak power. Even though the second term is very similar to that of TPA, TPA usually does not occur along with single photon absorption, whereas ESA can.

The fitting results are shown in Figure 4a and all the fitted parameters are summarized in Table 1. Only the fittings at polarization angles from 100° to 180° (from the minimum to the maximum normalized absorbance in Figure 2b) are shown, which roughly align with the a -axis and b -axis shown in Figure 1a, respectively. The fitted linear absorption coefficients at different angles (Table 1) agree well with those obtained from linear absorption measurement shown in Figure 2d, with only about 3% deviation, which validates our model. Both the linear absorption coefficient (α_0) and ESA coefficient (β_0) decrease with polarization angle. With larger linear absorption coefficient, density of excited carriers on state S2 is larger. Considering the fact that S2 is actually the initial state of ESA, larger carrier density on S2 will increase the probability of optical transition from S2 to S3. It should not be surprising to see that β_0 follows the same trend as α_0 with polarization angle. Even though the fitted saturation peak power for SA ($I_{\alpha, \text{sat}}$) is much larger than that of ESA ($I_{\beta, \text{sat}}$), they both increase with the polarization angle. In Figure 4b, we plot the absorption coefficient terms for SA, ESA, and total absorption separately at different polarization angles, based on the fitting results with Equation (1). It can be seen that both the SA and ESA show strong dependence on polarization angle. When the laser polarization

roughly aligns with a -axis, saturation effects from both single photon and excited-state absorption are clearly apparent. However, because the saturation of state S3 due to ESA occurs at very low laser peak power, SA at state S2 dominates the total absorption. When the laser polarization aligns with the b -axis (parallel to Re-atom chain), SA at state S2 disappears. Saturation of state S3 still occurs, but at much higher laser peak power. ESA dominates the change of total absorption coefficients with laser peak power.

We now consider the origin of this anisotropic response. Saturation peak power of certain energy states (S2 or S3 in our case) depend on two factors: transition probability from S1 to S2 (or S2 to S3) and density of states (DOS), the latter of which determines the capacity of S2 (or S3) to accommodate carriers. Transition probability could be obtained from first-principles calculations, but we are not aware of any report about transition probability of ReS₂ in literature. To some extent, the absorption coefficient for SA (α_0) and ESA (β_0) can reflect the transition probability at different polarization angles. Smaller coefficients at larger polarization angles indicate it is more difficult for the optical transition to occur. The DOS is defined as the available number of states per energy interval, which is related to the electronic band structure. One recent experimental study with angle-resolved photoemission (ARPES) found that the valence band of ReS₂ consists of many narrow mini bands that are anisotropic, and most dispersive along the Re-chain direction (b -axis).^[65] If a similar trend applies to the conduction band, we can expect that the DOS along the b -axis is larger. Both the smaller transition probability and larger DOS along b -axis could then contribute to the larger saturation laser peak power for S2 and S3.

3. Conclusion

We have measured the polarization-dependent reflection and transmission in bulk ReS₂, from which we have deduced the absorption and extracted the absorption coefficients with transfer matrix method. Absorption coefficients under high laser power show a transition from SA to RSA when rotating the laser polarization with respect to the b -axis. We further utilized the I-scan technique to measure the polarization-dependent nonlinear process in ReS₂ and found that both saturable and excited-state absorption contribute to the observed absorption coefficient change with laser power. Both the SA and ESA show strong dependence on the polarization angle, which we attribute to the anisotropic optical transition probability and electronic band structure in ReS₂. The anisotropic SA and ESA with polarization angle suggest potential application of ReS₂ as a saturable absorber in Q-switch or passive mode-locking lasers. For lasers operating with primary wavelength coinciding with direct transition band edge (Exciton II in this case), ESA is not desirable. The ESA saturation fluence of ReS₂ at 100° (1.75 mJ cm^{-2}) is comparable to other 2D TMDs (2 mJ cm^{-2} for black phosphorus,^[67] 2.5 mJ cm^{-2} for MoS₂,^[68] and 5.6 mJ cm^{-2} for WS₂,^[68]), while much smaller than traditional saturable absorbers, such as Cr⁴⁺:LuAG (18 mJ cm^{-2}), Cr⁴⁺:YSGG (45 mJ cm^{-2}), and Cr⁴⁺:YAG (68 mJ cm^{-2}).^[69] Small saturation power of ESA in ReS₂ along the a -axis will minimize

Table 1. Fitting parameters for linear/excited-state absorption coefficients and saturation terms based on Equation (1).

Polarization [°]	α_0 [cm ⁻¹]	$I_{\alpha, \text{sat}}$ [GW cm ⁻²]	β_0 [cm GW ⁻¹]	$I_{\beta, \text{sat}}$ [GW cm ⁻²]
100	29 300 ± 440	500 ± 71	160 ± 218	5 ± 2.5
120	30 200 ± 480	547 ± 90	170 ± 214	6.3 ± 3.1
140	29 500 ± 220	1800 ± 461	150 ± 76	9.56 ± 2.4
150	29 500 ± 119	6000 ± 561	70 ± 23.8	22 ± 7
160	29 000 ± 91	7822 ± 2071	50 ± 11	40 ± 18
180	27 000 ± 75	182000 ± 16717	33.6 ± 9.6	50 ± 34

the absorption loss due to ESA and hence provides a unique advantage. Along the *b*-axis, where SA is suppressed, it may be possible to utilize the ESA effect in ReS₂ for upconversion lasers, for example, pumping with photon energy of state S2 while lasing at photon energy of state S3. Even though only bulk ReS₂ sample is studied, this anisotropic nonlinear optical phenomenon is expected to also occur in few-layer and mono-layer samples, due to the relatively weak interlayer coupling in ReS₂.

Supporting Information

Supporting Information is available from the Wiley Online Library or from the author.

Acknowledgements

X.M. and Y.Z. contributed equally to this work. The authors would like to acknowledge support from National Science Foundation (NASCENT, Grant No. EEC-1160494; CAREER, Grant No. CBET-1351881); Department of Energy (SBIR/STTR, Grant No. DE-SC0013178); and DOD Army (Grant No. W911NF-16-1-0559).

Conflict of Interest

The authors declare no conflict of interest.

Keywords

intensity-scan technique, nonlinear optics, polarization, rhenium disulfide, saturable absorption, transition metal dichalcogenides

Received: February 2, 2018

Revised: March 26, 2018

Published online:

- [1] A. K. Geim, K. S. Novoselov, *Nat. Mater.* **2007**, *6*, 183.
- [2] K. I. Bolotin, K. Sikes, Z. Jiang, M. Klima, G. Fudenberg, J. Hone, P. Kim, H. Stormer, *Solid State Commun.* **2008**, *146*, 351.
- [3] M. Bernardi, M. Palumbo, J. C. Grossman, *Nano Lett.* **2013**, *13*, 3664.
- [4] R. R. Nair, P. Blake, A. N. Grigorenko, K. S. Novoselov, T. J. Booth, T. Stauber, N. M. Peres, A. K. Geim, *Science* **2008**, *320*, 1308.
- [5] K. F. Mak, K. He, J. Shan, T. F. Heinz, *Nat. Nanotechnol.* **2012**, *7*, 494.
- [6] B. Zhu, H. Zeng, J. Dai, Z. Gong, X. Cui, *Proc. Natl. Acad. Sci. USA* **2014**, *111*, 11606.
- [7] X. Xu, W. Yao, D. Xiao, T. F. Heinz, *Nat. Phys.* **2014**, *10*, 343.
- [8] Z. Zhu, Y. Cheng, U. Schwingenschlöggl, *Phys. Rev. B* **2011**, *84*, 153402.
- [9] Y.-M. Lin, K. A. Jenkins, A. Valdes-Garcia, J. P. Small, D. B. Farmer, P. Avouris, *Nano Lett.* **2008**, *9*, 422.
- [10] B. Radisavljevic, A. Radenovic, J. Brivio, I. V. Giacometti, A. Kis, *Nat. Nanotechnol.* **2011**, *6*, 147.
- [11] W. Zhao, R. M. Ribeiro, M. Toh, A. Carvalho, C. Kloc, A. Castro Neto, G. Eda, *Nano Lett.* **2013**, *13*, 5627.
- [12] K. F. Mak, C. Lee, J. Hone, J. Shan, T. F. Heinz, *Phys. Rev. Lett.* **2010**, *105*, 136805.
- [13] H. Murray, S. Kelty, R. Chianelli, C. Day, *Inorg. Chem.* **1994**, *33*, 4418.
- [14] K. Dileep, R. Sahu, S. Sarkar, S. C. Peter, R. Datta, *J. Appl. Phys.* **2016**, *119*, 114309.
- [15] S. Tongay, H. Sahin, C. Ko, A. Luce, W. Fan, K. Liu, J. Zhou, Y.-S. Huang, C.-H. Ho, J. Yan, *Nat. Commun.* **2014**, *5*, 3252.
- [16] O. B. Aslan, D. A. Chenet, A. M. van der Zande, J. C. Hone, T. F. Heinz, *ACS Photonics* **2015**, *3*, 96.
- [17] C. Ho, Y. Huang, K. Tiong, P. Liao, *J. Phys.: Condens. Matter* **1999**, *11*, 5367.
- [18] E. Zhang, Y. Jin, X. Yuan, W. Wang, C. Zhang, L. Tang, S. Liu, P. Zhou, W. Hu, F. Xiu, *Adv. Funct. Mater.* **2015**, *25*, 4076.
- [19] C. Ho, C. Huang, *J. Alloys Compd.* **2004**, *383*, 74.
- [20] C. Ho, Y. Huang, K. Tiong, *J. Alloys Compd.* **2001**, *317*, 222.
- [21] M. Gehlmann, I. Aguilera, G. Bihlmayer, S. Nemsák, P. Nagler, P. Gospodarič, G. Zamborlini, M. Eschbach, V. Feyer, F. Kronast, E. Mhryczak, T. Korn, L. Plucinski, C. Schüller, S. Blügel, C. M. Schneider, *Nano Lett.* **2017**, *17*, 5187.
- [22] H. Zhao, J. Wu, H. Zhong, Q. Guo, X. Wang, F. Xia, L. Yang, P. Tan, H. Wang, *Nano Res.* **2015**, *8*, 3651.
- [23] P. Nagler, G. Plechinger, C. Schüller, T. Korn, *Phys. Status Solidi RRL* **2016**, *10*, 185.
- [24] R. He, J.-A. Yan, Z. Yin, Z. Ye, G. Ye, J. Cheng, J. Li, C. Lui, *Nano Lett.* **2016**, *16*, 1404.
- [25] E. Lorchat, G. Froehlicher, S. Berciaud, *ACS Nano* **2016**, *10*, 2752.
- [26] H. Jang, C. R. Ryder, J. D. Wood, M. C. Hersam, D. G. Cahill, *Adv. Mater.* **2017**, *29*, 1700650.
- [27] Y.-C. Lin, H.-P. Komsa, C.-H. Yeh, T. Bjorkman, Z.-Y. Liang, C.-H. Ho, Y.-S. Huang, P.-W. Chiu, A. V. Krasheninnikov, K. Suenaga, *ACS Nano* **2015**, *9*, 11249.
- [28] C. Ho, H. Lee, C. Wu, *J. Phys.: Condens. Matter* **2004**, *16*, 5937.
- [29] F. Liu, S. Zheng, X. He, A. Chaturvedi, J. He, W. L. Chow, T. R. Mion, X. Wang, J. Zhou, Q. Fu, *Adv. Funct. Mater.* **2016**, *26*, 1169.
- [30] X. Wang, A. M. Jones, K. L. Seyler, V. Tran, Y. Jia, H. Zhao, H. Wang, L. Yang, X. Xu, F. Xia, *Nat. Nanotechnol.* **2015**, *10*, 517.
- [31] J. Qiao, X. Kong, Z.-X. Hu, F. Yang, W. Ji, *Nat. Commun.* **2014**, *5*.
- [32] H. Yuan, X. Liu, F. Afshinmanesh, W. Li, G. Xu, J. Sun, B. Lian, A. G. Curto, G. Ye, Y. Hikita, *Nat. Nanotechnol.* **2015**, *10*, 707.
- [33] S. Sim, D. Lee, M. Noh, S. Cha, C. H. Soh, J. H. Sung, M.-H. Jo, H. Choi, *Nat. Commun.* **2016**, *7*, 13569.
- [34] R. Wei, H. Zhang, X. He, Z. Hu, X. Tian, Q. Xiao, Z. Chen, J. Qiu, *Opt. Mater. Express* **2015**, *5*, 1807.
- [35] E. M. Mannebach, K.-A. N. Duerloo, L. A. Pellouchoud, M.-J. Sher, S. Nah, Y.-H. Kuo, Y. Yu, A. F. Marshall, L. Cao, E. J. Reed, *ACS Nano* **2014**, *8*, 10734.
- [36] X. Zheng, Y. Zhang, R. Chen, Z. Xu, T. Jiang, *Opt. Express* **2015**, *23*, 15616.
- [37] Y. Cui, F. Lu, X. Liu, *Sci. Rep.* **2017**, *7*.
- [38] Q. Cui, R. A. Muniz, J. Sipe, H. Zhao, *Phys. Rev. B* **2017**, *95*, 165406.
- [39] M. Sheik-Bahae, A. A. Said, T.-H. Wei, D. J. Hagan, E. W. Van Stryland, *IEEE J. Quantum Electron.* **1990**, *26*, 760.
- [40] K. G. Zhou, M. Zhao, M. J. Chang, Q. Wang, X. Z. Wu, Y. Song, H. L. Zhang, *Small* **2015**, *11*, 694.
- [41] H. Long, L. Tao, C. Y. Tang, H. Y. Tam, Q. Wen, Y. H. Tsang, *J. Mater. Chem. C* **2016**, *4*, 678.
- [42] K. Wang, Y. Feng, C. Chang, J. Zhan, C. Wang, Q. Zhao, J. N. Coleman, L. Zhang, W. J. Blau, J. Wang, *Nanoscale* **2014**, *6*, 10530.
- [43] I. Dancus, V. Vlad, A. Petris, T. B. Rujoiu, I. Rau, F. Kajzar, A. Meghea, A. Tane, *Rom. Rep. Phys.* **2013**, *65*, 966.
- [44] Q. Yang, J. Seo, S. J. Creekmore, D. A. Temple, K. Yoo, S. Kim, S. Jung, A. G. Mott, *Proc. SPIE 4797, Multiphoton Absorption and Nonlinear Transmission Processes: Materials, Theory, and Applications*, Seattle, WA, USA, February **2003**.
- [45] B. Taheri, H. Liu, B. Jassemnejad, D. Appling, R. C. Powell, J. Song, *Appl. Phys. Lett.* **1996**, *68*, 1317.

- [46] Y. Li, N. Dong, S. Zhang, X. Zhang, Y. Feng, K. Wang, L. Zhang, J. Wang, *Laser Photonics Rev.* **2015**, *9*, 427.
- [47] D. A. Chenet, O. B. Aslan, P. Y. Huang, C. Fan, A. M. van der Zande, T. F. Heinz, J. C. Hone, *Nano Lett.* **2015**, *15*, 5667.
- [48] C. Ho, Y. Huang, K. Tiong, P. Liao, *Phys. Rev. B* **1998**, *58*, 16130.
- [49] C. Ho, P. Liao, Y. Huang, T.-R. Yang, K. Tiong, *J. Appl. Phys.* **1997**, *81*, 6380.
- [50] X.-F. Qiao, J.-B. Wu, L. Zhou, J. Qiao, W. Shi, T. Chen, X. Zhang, J. Zhang, W. Ji, P.-H. Tan, *Nanoscale* **2016**, *8*, 8324.
- [51] C. C. Katsidis, D. I. Siapkas, *Appl. Opt.* **2002**, *41*, 3978.
- [52] K. Friemelt, L. Kulikova, L. Kulyuk, A. Siminel, E. Arushanov, C. Kloc, E. Bucher, *J. Appl. Phys.* **1996**, *79*, 9268.
- [53] Q. Cui, J. He, M. Z. Bellus, M. Mirzokarimov, T. Hofmann, H. Y. Chiu, M. Antonik, D. He, Y. Wang, H. Zhao, *Small* **2015**, *11*, 5565.
- [54] R. G. Driggers, *Encyclopedia of Optical Engineering: Las-Pho*, Vol. 2, CRC Press, Boca Raton, FL **2003**, p. 1025.
- [55] A. Tiwari, *Innovative Graphene Technologies: Evaluation and Applications*, Vol. 2, Smithers Rapra, Shrewsbury, UK **2013**.
- [56] S. Zhang, N. Dong, N. McEvoy, M. O'Brien, S. Winters, N. C. Berner, C. Yim, Y. Li, X. Zhang, Z. Chen, *ACS Nano* **2015**, *9*, 7142.
- [57] K. Wang, J. Wang, J. Fan, M. Lotya, A. O'Neill, D. Fox, Y. Feng, X. Zhang, B. Jiang, Q. Zhao, *ACS Nano* **2013**, *7*, 9260.
- [58] H. Yang, X. Feng, Q. Wang, H. Huang, W. Chen, A. T. Wee, W. Ji, *Nano Lett.* **2011**, *11*, 2622.
- [59] J. Sotor, G. Sobon, W. Macherzynski, P. Paletko, K. M. Abramski, *Appl. Phys. Lett.* **2015**, *107*, 051108.
- [60] A. Penzkofer, J. Wiedmann, *Opt. Commun.* **1980**, *35*, 81.
- [61] K. D. Belfield, M. V. Bondar, I. Cohanoschi, F. E. Hernandez, O. D. Kachkovsky, O. V. Przhonska, S. Yao, *Appl. Opt.* **2005**, *44*, 7232.
- [62] P. Morkel, R. I. Laming, *Opt. Lett.* **1989**, *14*, 1062.
- [63] Z. Burshtein, P. Blau, Y. Kalisky, Y. Shimony, M. Kikta, *IEEE J. Quantum Electron.* **1998**, *34*, 292.
- [64] C. Ho, Y. Huang, J. Chen, T. Dann, K. Tiong, *Phys. Rev. B* **1999**, *60*, 15766.
- [65] D. Biswas, A. M. Ganose, R. Yano, J. Riley, L. Bawden, O. Clark, J. Feng, L. Collins-Mcintyre, M. Sajjad, W. Meevasana, *Phys. Rev. B* **2017**, *96*, 085205.
- [66] Q. Ouyang, H. Yu, K. Zhang, Y. Chen, *J. Mater. Chem. C* **2014**, *2*, 6319.
- [67] D. Li, H. Jussila, L. Karvonen, G. Ye, H. Lipsanen, X. Chen, Z. Sun, *Sci. Rep.* **2015**, *5*, 15899.
- [68] S. Zhang, L. Guo, M. Fan, F. Lou, P. Gao, H. Lv, X. Wang, J. Yang, T. Li, K. Yang, *IEEE Photonics J.* **2017**, *9*, 1.
- [69] Y. Kalisky, *Prog. Quantum Electron.* **2004**, *28*, 249.